Inorganic Chemistry

ARTICLE

pubs.acs.org/IC

Complete Titanium Substitution by Boron in a Tetragonal Prism: Exploring the Complex Boride Series $Ti_{3-x}Ru_{5-y}Ir_yB_{2+x}$ ($0 \le x \le 1$ and $1 < y < 3$) by Experiment and Theory

Boniface P. T. Fokwa* and Martin Hermus

Institute of Inorganic Chemistry, RWTH Aachen University, D-52056 Aachen, Germany

Supporting Information

ABSTRACT: Polycrystalline samples and single crystals of four members of the new complex boride series $Ti_{3-x}Ru_{5-y}Ir_yB_{2+x}$ ($0 \le x \le 1$ and $1 < y < 3$) were synthesized by arc-melting the elements in a water-cooled copper crucible under an argon atmosphere. The new silvery phases were structurally characterized by powder and single-crystal X-ray diffraction as well as energy- and wavelength-dispersive X-ray spectroscopy analyses. They crystallize with the tetragonal $Ti_3Co_5B_2$ structure type in space group $P4/mbm$ (No. 127). Tetragonal prisms of Ru/Ir atoms are filled with titanium in the boron-poorest phase ($Ti_3Ru_{2.9}Ir_{2.1}B_2$). Gradual substitution of titanium by boron then results in the successive filling of this site by a Ti/B mixture en route to the complete boron occupation, leading to the boron-richest phase ($Ti_2Ru_{2.8}Ir_{2.2}B_3$). Furthermore, both ruthenium and iridium share two sites in these structures, but a clear Ru/Ir site preference is found. First-principles density functional theory calculations (Vienna ab initio simulation package) on appropriate structural models (using a supercell approach) have provided more evidence on the stability of the boron-richest and -poorest phases, and the calculated lattice parameters corroborate very well with the experimentally found ones. Linear muffin-tin orbital atomic sphere approximation calculations further supported these findings through crystal orbital Hamilton population bonding analyses, which also show that the Ru/Ir−B and Ru/Ir−Ti heteroatomic interactions are mainly responsible for the structural stability of these compounds. Furthermore, some stable and unstable phases of this complex series could be predicted using the rigid-band model. According to the density of states analyses, all phases should be metallic conductors, as was expected from these metal-rich borides.

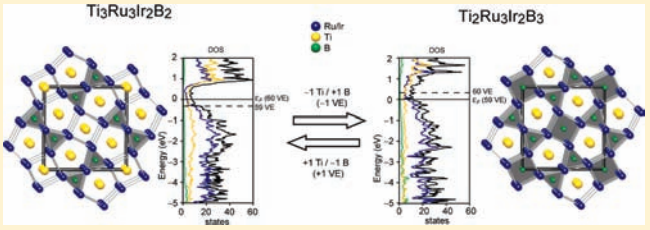

1. INTRODUCTION

Within the last 2 decades, ordered substitutional variants of the $Ti_3Co_5B_2$-type structure[1] with the general composition $A_2MT_5B_2$ (A = Mg, Sc; M = main-group and 3d elements; T = Ru, Rh, Ir) have been intensely investigated both experimentally and theoretically, in particular with respect to itinerant magnetism.[2−6] These phases exhibit a truly outstanding structural unit, namely, well-separated chains of magnetic 3d atoms (M) with intrachain and interchain distances of about 3.0 and 6.6 Å, respectively. In these earlier investigations, the two T sites present in the crystal structures of the $A_2MT_5B_2$ phases have been occupied by either a 4d or a 5d transition metal. A mixture of different 4d transition metals was also reported [for example, in the $A_2FeRu_{5-n}Rh_nB_2$ (A = Sc, Zr) series],[6] but no phase containing a 4d/5d mixture was known. This is surprising because from an X-ray diffraction point of view it should be easier to distinguish a 4d/5d mixture than a 4d/4d mixture, provided, of course, there is a successful synthesis. Therefore, the synthesis and structural characterization of compounds adopting the $Ti_3Co_5B_2$-type structure and containing this 4d/5d mixture is one of the objectives of this work. This implies a 4d/5d site preference study on the available sites in the crystal structures. Another important aspect of the $Ti_3Co_5B_2$-type structure is its structural flexibility, in particular with respect to the M site of the substitutional variant $A_2MT_5B_2$. In fact, this M site can accommodate a large variety of elements, ranging from small main-group elements (e.g., Be) to large transition metals (e.g., Sc).[2−4] This flexibility is further tested in this work because a successive substitution of titanium at the M site by the much smaller boron will be tried, en route to the discovery of an unprecedented phase where boron would occupy the M position and therefore be surrounded by eight neighbors in a tetragonal-prismatic coordination. Another unusual substitution of a transition metal (rhodium) by boron was reported in the boride phase $Mg_2Rh_{1-x}B_{6+2x}$.[7] For these studies, single-crystal structural analysis is desirable, in particular because of a possible 4d/5d site preference but also for the localization of boron sites in the boron-richer phase. From a theoretical perspective, first-principles density functional theory (DFT) calculations on appropriate structural models will be used to probe the stability of these phases with respect to their boron content.

2. EXPERIMENTAL SECTION

2.1. Synthesis and Characterization. Single crystals of the series $Ti_{3-x}Ru_{5-y}Ir_yB_{2+x}$ ($x = 0−1$ and $y = 1.6−2.7$) were synthesized

Received: October 25, 2010
Published: March 23, 2011

Table 1. Crystallographic and Structure Refinement Data of $Ti_3Ru_{2.9(2)}Ir_{2.1(2)}B_2$, $Ti_{2.63(4)}Ru_{3.4(2)}Ir_{1.6(2)}B_{2.37(4)}$, $Ti_{2.27(6)}Ru_{2.5(2)}Ir_{2.5(2)}B_{2.73(6)}$, and $Ti_2Ru_{2.8(2)}Ir_{2.2(2)}B_3$

	$Ti_3Ru_{2.9}Ir_{2.1}B_2$	$Ti_{2.63}Ru_{3.4}Ir_{1.6}B_{2.37}$	$Ti_{2.27}Ru_{2.5}Ir_{2.5}B_{2.73}$	$Ti_2Ru_{2.8}Ir_{2.2}B_3$
fw ($g\cdot mol^{-1}$) ; $F(000)$	859.31; 729	804.12; 686	871.60; 732	838.62; 707
crystal size (mm^3)	0.05 × 0.02 × 0.02	0.06 × 0.03 × 0.02	0.07 × 0.03 × 0.03	0.04 × 0.01 × 0.01
space group; Z	*P*4/*mbm* (No. 127); 2			
lattice parameters				
a (Å)	9.236(5)	9.180(3)	9.149(4)	9.030(2)
c (Å)	2.972(2)	2.944(2)	2.928(2)	2.855(2)
V ($Å^3$)	253.5(3)	248.1(2)	245.1(2)	232.8(1)
calcd density ($g\cdot cm^{-3}$)	11.26	10.76	11.81	11.96
abs corrn	semiempirical			
abs coeff (mm^{-1})	66.88	56.97	84.21	75.79
T_{min}; T_{max}	0.135; 0.348	0.131; 0.395	0.067; 0.187	0.152; 0.518
diffractometer	Bruker APEX CCD, Mo Kα, graphite monochromator			
θ range (deg)	4.94−35.96	4.97−35.59	4.98−35.53	5.05−35.90
hkl range	$-11 \le h \le 8$	$-15 \le h \le 13$	$-11 \le h \le 14$	$-14 \le h \le 14$
	$-8 \le k \le 15$	$-14 \le k \le 14$	$-14 \le k \le 14$	$-14 \le k \le 14$
	$-4 \le l \le 4$	$-4 \le l \le 4$	$-4 \le l \le 4$	$-4 \le l \le 4$
no. of reflns; R_{int}	1245; 0.0755	3162; 0.0928	2439; 0.1199	4560; 0.0563
no. of indep reflns	355	346	338	337
no. of param	26	22	28	27
refinement	*SHELX-97*, full matrix against F^2			
R1; wR2 [$I > 2\sigma(I)$]	0.0607; 0.1170	0.0480; 0.1054	0.0721; 0.1451	0.0390; 0. 0885
R1; wR2 (all I)	0.0942; 0.1284	0.0718; 0.1154	0.1162; 0.1635	0.0412; 0. 0896
GOF	1.072	1.071	1.116	1. 052
diff. peak/hole ($e\cdot Å^{-3}$)	4.232/−3.678	3.312/−2.901	4.801/−3.923	4.276/−3.362

by arc-melting the elements in a water-cooled copper crucible under an argon atmosphere using a tungsten tip as the second electrode. The starting elements, titanium (pieces, 99.9%, Degussa), ruthenium (powder, 99.9%, Chempur), iridium (powder, 99.9%, Chempur), and boron (amorphous powder, 97%, ABCR, or crystalline pieces, 99.999% Alfa Aesar), were weighed in the respective atomic ratios according to the hypothetical formulas $Ti_3Ru_3Ir_2B_2$, $Ti_{2.5}Ru_3Ir_2B_{2.5}$, and $Ti_2Ru_3Ir_2B_3$. The boron-richest phase could be achieved after using an excess of 10% boron. The well-homogenized reactants were pressed into pellets. They were then melted at least three times (for ca. 10 s each) by an electric arc argon plasma at a direct current of 40 A. Each time the sample was turned over before remelting to gain a homogeneous product. The argon was purified over silica gel, molecular sieves, and titanium sponge (950 K). Weight losses during the melting process were below 1%. Silvery products with metallic luster containing some single crystals suitable for X-ray structural analysis were obtained. Four needle-shaped single crystals (one from $Ti_3Ru_3Ir_2B_2$, one from $Ti_2Ru_3Ir_2B_3$, and two others from $Ti_{2.5}Ru_3Ir_2B_{2.5}$ starting compositions) could be isolated manually under an optical microscope. Powder diffractograms of the products were taken using a Guinier powder diffractometer with Cu $K\alpha_1$ radiation (λ = 1.54059 Å) and silicon as an internal standard. Phase analysis and lattice parameter refinements were carried out using the program *WINXPOW*.[8]

The presence of the three metals and their ratios were routinely characterized by energy-dispersive X-ray spectroscopy (EDS) analysis first, using a high-resolution, low-energy scanning electron microscope of the type LEO 1530 (Oberkochen, Germany) equipped with an EDS system of the type INCA (Oxford, England). EDS measurements on several selected crystals provided Ti/Ru/Ir ratios of 1:1.06:0.65 (averaged experimental data) for the boron-poorest phase and 1:1.48:1.02 for the boron-richest phase. For the intermediate starting composition, the crystals used show a strong variation of the Ru/Ir ratio, inducing a range of the Ti/Ru/Ir ratio between 1:1.32:0.64 and 1:1.04:1.25 and thus leading to a phase width that was also confirmed by powder and single-crystal X-ray analyses. It is worth mentioning that the metal compositions obtained from the single-crystal refinements were confirmed by these EDS measurements. Additionally, the boron-poorer and -richer compositions were analyzed by wavelength-dispersive X-ray spectroscopy (WDS) on polished surfaces of the synthesized samples using a CAMEBAX SX 50 electron probe X-ray analyzer (year 1991, equipped with four wavelength-dispersive X-ray spectrometers). Single-crystalline elemental boron was used as the standard for boron analysis. The compositions found, $Ti_{3.0(3)}Ru_{2.8(2)}Ir_{2.0(1)}B_{2.2(4)}$ and $Ti_{2.0(2)}Ru_{2.8(1)}Ir_{2.3(2)}B_{2.9(2)}$, are within standard deviation in good agreement with the single-crystal results (see Single-Crystal Structure Refinement section). For the intermediate composition $Ti_{2.5}Ru_3Ir_2B_{2.5}$, although the WDS measurements of the two single crystals used could not yield a quantitative boron analysis, they confirmed the presence of boron and the absence of other light elements (C, N, and O).

2.2. Crystal Structure Determination. Single crystals of suitable sizes (see Table 1) were fixed on top of glass capillaries, and X-ray data were collected on a CCD single-crystal diffractometer (Bruker SMART APEX) with graphite-monochromatized Mo Kα radiation (λ = 0.710 73 Å). The X-ray intensities were corrected with respect to absorption using a semiempirical procedure.[9] The crystal structures were solved by means of direct methods and refined by full-matrix least-squares refinement[10] (based on F^2) using anisotropic displacement parameters (ADPs) for the heavy metals and an isotropic one for boron (Table 1). The obtained crystal structure data were then standardized using the program *STRUCTURE TIDY*.[11] A listing of the refinement data and data collection is available. [More details on the structure determinations may be obtained from the Fachinformationszentrum Karlsruhe (e-mail:

dx.doi.org/10.1021/ic102148x |*Inorg. Chem.* 2011, 50, 3332–3341

crysdata@fiz-karlsruhe.de), D-76344 Eggenstein-Leopoldshafen, Germany, on quoting the CSD depository numbers 420704 for $Ti_3Ru_{2.9}Ir_{2.1}B_2$, 422237 for $Ti_{2.63}Ru_{3.4}Ir_{1.6}B_{2.37}$, 422236 for $Ti_{2.27}Ru_{2.5}Ir_{2.5}B_{2.73}$, and 420705 for $Ti_2Ru_{2.8}Ir_{2.2}B_3$.]

2.3. Experimental Results and Discussion. *Phase Analysis.* Analysis of all powder diffractograms confirmed the isotypism of all phases with the $Ti_3Co_5B_2$-type structure. For the starting compositions $Ti_3Ru_3Ir_2B_2$ and $Ti_2Ru_3Ir_2B_3$, small amounts of Ti_xRu_{1-x} and $TiIr_3B_x$ phases could be identified as side products. Nevertheless, the yield of the main phase could be estimated in each case to be more than 90% (see, for example, the Rietveld refinement plot of $Ti_3Ru_3Ir_2B_2$ in Figure S1 of the Supporting Information). From these powder diffraction data, the peaks of the main phase were identified (see Tables S1 and S2 of the Supporting Information) and the subsequent refinement using the space group *P*4/*mbm* yielded the lattice parameters $a = 9.2459(4)$ Å, $c = 2.9751(2)$ Å, and $V = 254.33(1)$ Å^3 for $Ti_3Ru_3Ir_2B_2$ and $a = 9.0690(9)$ Å, $c = 2.8649(3)$ Å, and $V = 235.63(6)$ Å^3 for $Ti_2Ru_3Ir_2B_3$. The volume difference is very high ($\Delta V = 18.7$ Å^3), and the intensity distributions of both powder patterns are different, suggesting indeed that the compositions from both syntheses should be different, although both phases contain the same elements and are isostructural ($Ti_3Co_5B_2$ structure type). The fact that only titanium and boron have different stoichiometries in both starting compositions already indicates that one boron atom may have substituted a titanium atom in the titanium-richer phase, leading to this drastic decrease of the cell volume. Furthermore, the lattice parameters obtained from the single-crystal structural analyses (see Table 1) were in good agreement with the values obtained from the powder data in both the $Ti_3Ru_3Ir_2B_2$ and $Ti_2Ru_3Ir_2B_3$ cases, not only confirming the $Ti_3Co_5B_2$-type structure for the selected single crystals but also indicating a negligible phase width, in accordance with EDS and WDS measurements. Because a titanium substitution by boron is somewhat surprising, an intermediate composition, $Ti_{2.5}Ru_3Ir_2B_{2.5}$, was also synthesized in order to allow both titanium and boron to share the same site. The resulting powder diffractogram clearly confirmed the $Ti_3Co_5B_2$-type structure; however, much wider peaks were observed, indicating a phase width that was confirmed by both EDS analysis (see the Experimental Section) and single-crystal refinements (see below). Because this type of powder sample is not appropriate for lattice parameter refinement, these have to be determined using single crystals. Two suitable single crystals of the main phase ($Ti_3Co_5B_2$ structure type) were found in this product, and the refined cell volumes were significantly different (see Table 1). This suggests that different chemical formulas have to be expected, thereby further supporting the presence of a phase width. The determined cell volumes lie between those of the aforementioned boron-poorest and -richest phases, a clear indication that titanium is gradually substituted by boron throughout the $Ti_{3-x}Ru_3Ir_2B_{2+x}$ series.

Single-Crystal Structure Refinement. The lattice parameters and space group determination from the single-crystal analysis have confirmed isotypism ($Ti_3Co_5B_2$ structure type) for all phases (see Table 1). A detailed structure refinement is given for the $Ti_3Ru_3Ir_2B_2$ case, where titanium and boron are expected to fill their respective sites in the $Ti_3Co_5B_2$ structure type, with ruthenium and iridium having to share the cobalt sites (8j and 2c). The differences between this refinement and those of the $Ti_{2.5}Ru_3Ir_2B_{2.5}$ and $Ti_2Ru_3Ir_2B_3$ phases will then be elucidated.

For the $Ti_3Ru_3Ir_2B_2$ starting composition, all expected titanium and boron sites were found (4g and 2a for Ti and 4g for B) in the early stages of the refinement. However, neither ruthenium nor iridium could be safely refined on the two available sites (8j and 2c) because their ADPs were unsatisfactory. A significant improvement of the refinement was obtained by refining iridium on the Wyckoff site 8j and ruthenium on 2c, but the ADPs were still unacceptable. The ADPs of iridium were unusually large, whereas those of ruthenium were unusually small, suggesting less electron density on the iridium site and more on the ruthenium site. Both elements were then simultaneously refined on the two sites, leading to an immediate convergence of the refinement and to nearly the same ADPs on both sites (see Table 2). Because titanium and boron (or boron alone) could be refined at the Ti2 site (2a) in other phases (see below), we also tried a Ti/B mixed-occupancy refinement, but the refinement could not converge; therefore, titanium was again refined alone. A small electron density (ca. 6 e·Å^{-3}) was then localized at the vicinity of the 8j site and added to the refinement but restraining the site to full occupancy: The resulting occupancies for the 8j site were 0.49(3)/0.040(8) for Ru1a/Ru1b and 0.47(3) for Ir1. At the 2c site, the occupancies 0.80(3) for Ru2 and 0.20(3) for Ir2 were obtained, leading to the formula $Ti_3Ru_{2.9(2)}Ir_{2.1(2)}B_2$.

The lattice parameters of the two single crystals obtained for the $Ti_{2.5}Ru_3Ir_2B_{2.5}$ starting composition were so different (see Table 1) that two different chemical formulas were expected. The refinement procedure stated above was also conducted in both cases. Although a convergence of the refinement could be achieved, the ADPs of Ti2 (2a) were unexpectedly twice as large as those of Ti1. A mixed-occupancy refinement with titanium and boron on this 2a site was then successfully used, leading to well-improved reliability values. The final refinement cycles lead to two different formulas for the two single crystals, as expected: $Ti_{2.63(4)}Ru_{3.4(2)}Ir_{1.6(2)}B_{2.37(4)}$ and $Ti_{2.27(6)}Ru_{2.5-(2)}Ir_{2.5(2)}B_{2.73(6)}$. Furthermore, the displacement parameters of the Ti2/B2 site (2a) in the boron-poorer phase could be refined anisotropically, whereas they could only be safely refined isotropically in the boron-richer one because of the high boron percentage on this site (73%). Although each of the two above-mentioned chemical formulas differ greatly from the loaded composition, their average $Ti_{2.45}Ru_{2.95}Ir_{2.05}B_{2.55}$ is, however, very close to it.

Regarding the $Ti_2Ru_3Ir_2B_3$ starting composition, the boron content was further increased with the aim of achieving a 100% substitution of titanium by boron at the Ti2 site (2a). Indeed the same refinement procedure leads to a full occupation of this site by boron, and a Ti2/B2 mixed-occupancy refinement was unsuccessful. However, a disorder was also observed for the Ir1/Ru1 site and was successfully modeled to the occupancies given in Table 2. The final proper refinement, with isotropic displacement parameters for both B1 and B2 in the expected range, leads to the formula $Ti_2Ru_{2.8(2)}Ir_{2.2(2)}B_3$.

Structural Description. All of the four above-mentioned phases belong to the $Ti_{3-x}Ru_{5-y}Ir_yB_{2+x}$ complex boride series, which may be better understood as $Ti_2(Ti_{1-x}B_x)Ru_{5-y}Ir_yB_2$ ($0 \le x \le 1$ and $1 < y < 3$). They crystallize with the $Ti_3Co_5B_2$-type structure, space group *P*4/*mbm*, and represent the first members of the Ti−Ru−Ir−B system. They are also the first phases of the $Ti_3Co_5B_2$-type structure where a mixture of 4d with 5d transition metals is observed at the two cobalt sites (see Figure 1). Although the realization of a 4d/5d mixture is new, it is not very surprising, given the fact that quaternary derivatives ($A_2MT_5B_2$) of the $Ti_3Co_5B_2$-type structure are already known that contain either ruthenium or iridium at the T (or Co) sites, e.g., $Mg_2FeIr_5B_2$ and $Sc_2FeRu_5B_2$. Moreover, a 4d/4d mixture at these sites was also reported in $Sc_2MnRu_2Rh_3B_2$[5] and in the $A_2FeRu_{5-n}Rh_nB_2$ (A = Sc, Zr) series.[6]

The crystal structures of phases within the $Ti_{3-x}Ru_{5-y}Ir_yB_{2+x}$ complex boride series contain trigonal, tetragonal, and pentagonal prisms of the Ru/Ir atoms stacked on top of each other, thereby building channels along the [001] direction (see Figure 1). While boron atoms center the trigonal prisms in all phases, the titanium atoms are found in the pentagonal prisms. The tetragonal prisms are filled differently, depending on the Ti/B ratio. They are first filled by titanium atoms in $Ti_3Ru_{2.9}Ir_{2.1}B_2$ (Figure 1, left), then by a mixture of titanium and boron atoms in $Ti_{2.63}Ru_{3.4}Ir_{1.6}B_{2.37}$ and $Ti_{2.27}Ru_{2.5}Ir_{2.5}B_{2.73}$, and finally by boron atoms in $Ti_2Ru_{2.8}Ir_{2.2}B_3$ (Figure 1, right).

Ru/Ir Site Preference. Two Wyckoff sites (8j and 2c) are available for both ruthenium and iridium in the different structures within the

Table 2. Atomic Coordinates, Equivalent Isotropic Displacement Parameters U_{eq} (Å^2) for $Ti_3Ru_{2.9(2)}Ir_{2.1(2)}B_2$, $Ti_{2.63(4)}Ru_{3.4(2)}Ir_{1.6(2)}B_{2.37(4)}$, $Ti_{2.27(6)}Ru_{2.5(2)}Ir_{2.5(2)}B_{2.73(6)}$, and $Ti_2Ru_{2.8(2)}Ir_{2.2(2)}B_3$[a]

atom	Wyckoff position	occupation	x	y	z	U_{eq}
			$Ti_3Ru_{2.9(2)}Ir_{2.1(2)}B_2$			
Ru1a/Ir1/	8j	0.47(3)/0.49	0.0720(2)	0.2150(2)	$^1/_2$	0.0039(2)
Ru1b	16l	0.020(4)	0.118(6)	0.169(6)	0.35(2)	
Ru2/Ir2	2c	0.80(2)/0.20	0	$^1/_2$	$^1/_2$	0.0059(8)
Ti1	4g	1.0	0.1759(5)	0.6759(5)	0	0.008(2)
Ti2	2a	1.0	0	0	0	0.006(2)
B1	4g	1.0	0.622(3)	0.122(3)	0	0.009(6)
			$Ti_{2.63(4)}Ru_{3.4(2)}Ir_{1.6(2)}B_{2.37(4)}$			
Ru1/Ir1	8j	0.62(3)/0.38	0.07130(9)	0.21159(9)	$^1/_2$	0.0132(3)
Ru2/Ir2	2c	0.93(3)/0.07	0	$^1/_2$	$^1/_2$	0.0095(7)
Ti1	4g	1.0	0.1751(3)	0.6751(3)	0	0.015(2)
Ti2/B2	2a	0.63(4)/0.37	0	0	0	0.012(2)
B1	4g	1.0	0.626(2)	0.126(2)	0	0.020(5)
			$Ti_{2.27(6)}Ru_{2.5(2)}Ir_{2.5(2)}B_{2.73(6)}$			
Ru1/Ir1a/	8j	0.43(3)/0.55	0.0689(2)	0.2066(2)	$^1/_2$	0.0177(5)
Ir1b	16l	0.011(3)	0.060(8)	0.202(7)	0.87(2)	
Ru2/Ir2	2c	0.79(3)/0.21	0	$^1/_2$	$^1/_2$	0.013(1)
Ti1	4g	1.0	0.1755(5)	0.6755(5)	0	0.012(2)
Ti2/B2	2a	0.29(6)/0.71	0	0	0	0.011(6)
B1	4g	1.0	0.628(3)	0.128(3)	0	0.011(7)
			$Ti_2Ru_{2.8(2)}Ir_{2.2(2)}B_3$			
Ru1/Ir1a/	8j	0.50(3)/0.48/	0.06649(7)	0.20321(7)	$^1/_2$	0.0039(2)
Ir1b/Ir1c		0.013(2)/0.010(2)	0.037(4)/0.993(6)	0.139(5)/0.215(5)		
Ru2/Ir2	2c	0.74(3)/0.26	0	$^1/_2$	$^1/_2$	0.0029(4)
Ti1	4g	1.0	0.1761(3)	0.6761(3)	0	0.0073(8)
B2	2a	1.0	0	0	0	0.014(5)
B1	4g	1.0	0.629(2)	0.129(2)	0	0.010(3)

[a] U_{eq} is defined as $^1/_3$ of the trace of the orthogonalized U_{ij} tensors. For boron, $U_{eq} = U_{iso}$.

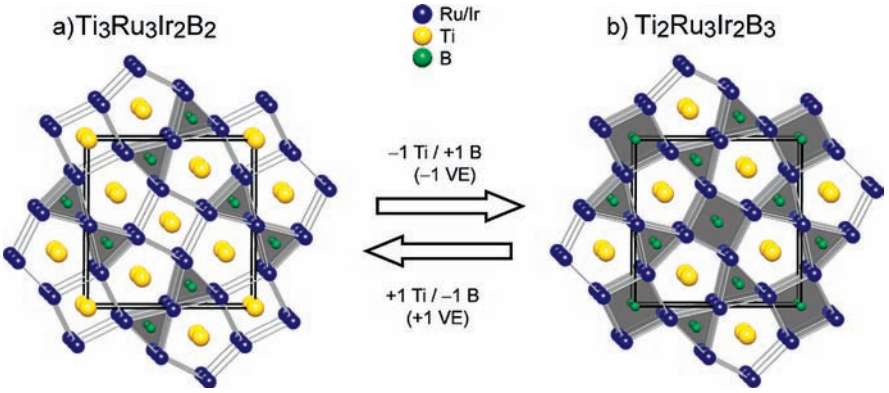

Figure 1. Projection nearly along [001] of the crystal structures of the two end members of the complex boride series $Ti_{3-x}Ru_{5-y}Ir_yB_{2+x}$ [$Ti_3Ru_{2.9}Ir_{2.1}B_2$ (a) and $Ti_2Ru_{2.8}Ir_{2.2}B_3$ (b)]. Boron-filled trigonal and tetragonal prisms are highlighted. One can switch from one phase to another by substituting titanium by boron, thereby removing one valence electron (VE) and thus decreasing the unit cell volume by 8.2%, or vice versa.

$Ti_{3-x}Ru_{5-y}Ir_yB_{2+x}$ series. Given the huge difference of the electron density between ruthenium and iridium, both are respectively 4d and 5d transition metals, a size-dependent site preference may be expected depending on the environment of the two sites. In the boron-poorer phase, the 8j site is surrounded by 12 metallic atoms and 2 boron ones in the form of a strongly distorted bicapped icosahedron (Figure 2a), whereas the 2c site is surrounded by 10 metallic atoms and 4 boron ones in the form of a slightly distorted bicapped icosahedron (Figure 2b). The question now is, which one (of both polyhedra) has the largest volume? A detailed inspection of both polyhedra (Figure 2) reveals that they differ from each other only on the Ru/Ir−Ti (2.57 Å, 8j polyhedron) and Ru/Ir−B (2.18 Å, 2c polyhedron) distances. This implies that the

dx.doi.org/10.1021/ic102148x |*Inorg. Chem.* 2011, 50, 3332–3341

icosahedron around 2c is smaller than that around 8j. Therefore, this volume difference between both polyhedra may drive a Ru/Ir size-dependent site preference. This Ru/Ir site preference is also expected in all phases of the $Ti_{3-x}Ru_{5-y}Ir_yB_{2+x}$ series containing both elements. Even in the boron-richer phase, the above-mentioned distances are 2.40 and 2.18 Å (see Figure 2), respectively, and thus are different enough to induce a significant volume difference between the two polyhedra. Because the atomic radius of ruthenium [r_a(Ru) = 1.32 Å, half the bonding distance in the ruthenium metal] is smaller than that of iridium [r_a(Ir) = 1.36 Å], it is expected that ruthenium will prefer the smaller polyhedron (2c site) and iridium the larger one (8j site). Indeed, throughout the $Ti_{3-x}Ru_{5-y}Ir_yB_{2+x}$ series, ruthenium is always found in excess [from 12pp (percentage points) up to 27pp] at the 2c site, whereas an excess of iridium (4pp to 12pp) is always observed at the 8j site (see Table 2). For example, in the phase $Ti_3Ru_{2.9(2)}Ir_{2.1(2)}B_2$, an occupation ratio of 58/42% for Ru/Ir is expected for each of the two sites, if a statistical distribution of both elements is assumed. However, 80/20% and 53/47% are found for Ru/Ir at the 2c and 8j sites, respectively, which means that 22pp ruthenium is found in excess on the 2c site, whereas 5pp more iridium is observed at the 8j site. Therefore, the smaller ruthenium prefers the smaller environment, as expected.

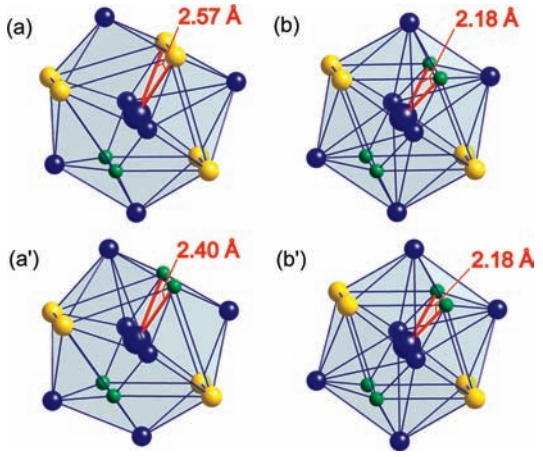

Figure 2. Polyhedra found around (Ru/Ir)1, 8j site (a and a′), and (Ru/Ir)2, 2c site (b and b′), in the crystal structures of the two end members of the complex boride series $Ti_{3-x}Ru_{5-y}Ir_yB_{2+x}$ [$Ti_3Ru_{2.9}Ir_{2.1}B_2$ (a and b) and $Ti_2Ru_{2.8}Ir_{2.2}B_3$ (a′ and b′)]. The highlighted distances are decisive for estimation of the polyhedron's volume: $V_a > V_b$; $V_{a'} > V_{b'}$; $V_a > V_{a'}$; $V_b \approx V_{b'}$.

Bonding Situation. Let us examine now the influence of a gradual titanium substitution by boron on the distances in the $Ti_{3-x}Ru_{5-y}Ir_yB_{2+x}$ series. The distances in the boride series follow the expected trend when the larger titanium [r_a(Ti) = 1.45 Å] in $Ti_3Ru_{2.9}Ir_{2.1}B_2$ is substituted by the smaller boron [r_a(B) = 0.79 Å] en route to $Ti_2Ru_{2.8}Ir_{2.2}B_3$. As expected, all distances around the X2 site (X2 = Ti2, Ti2/B2, or B2) directly affected by the substitution become smaller when the boron content increases (see Table 3). The trend of the remaining distances in the series is mostly dictated by the Ru/Ir ratio. The Ru/Ir−B1, Ru/Ir−Ti, and Ru/Ir−Ru/Ir distances are comparable with those present in the $Ti_{10}Ru_{19}B_8$,[12] $Ti_9M_2Ru_{18}B_8$,[13] and $Ti_{1.6}Os_{1.4}RuB_2$[14] phases, which contain at least three of the elements used. The Ru/Ir−B1 distances, which range from 2.18 Å to 2.21 Å in all phases, are in line with the Ru−B distances found in the above-mentioned compounds and are mainly responsible for the structural stability of these phases, as demonstrated by COHP bonding analysis (see the Theoretical Section). In $Ti_2Ru_{2.8}Ir_{2.2}B_3$, however, an additional Ru/Ir−B2 distance of 2.40 Å (8-fold boron coordination) is also found. This distance is larger than the previous Ru/Ir−B1 one, and thus weaker bonding should be expected. This assumption was also confirmed by COHP analysis (see the Theoretical Section). No Ru−B or Ir−B distance as long as 2.40 Å has been reported before in transition-metal borides of the $Ti_3Co_5B_2$ structure type. However, similar Ru−B (2.40 Å) and Ir−B (2.36 Å) distances are found in $Mo_{1.75}Ru_{1.25}B_2$[15] and Mo_2IrB_2[16], respectively. Furthermore, palladium, which is another transition metal having only a 0.02 Å larger atomic radius than iridium, was found to build beside the usual trigonal-prismatic coordination also a square-planar coordination around boron in the $Y_2Pd_{14}B_5$ phase with a larger Pd−B distance of 2.54 Å.[17a]

Boron Coordination by Transition Metals. The main question of this work remains: Is it possible to find boron atoms in tetragonal prisms of transition metals?

The additional boron atom found at a titanium site [in a $(Ru/Ir)_8$ tetragonal prism] in the boron-richest phase, $Ti_2Ru_{2.8}Ir_{2.2}B_3$, is surprising. To the best of our knowledge, such boron coordination has never been observed before. In fact, the most common boron coordination environments of transition metals are trigonal prisms and octahedra.[6c] However, boron is also found in unusual coordination environments of transition metals, like the square-planar boron coordination reported already for three different transition metals.[17] Polyhedra around boron with coordination numbers (CNs) higher than 6 have also been observed, namely, square antiprisms (CN 8) in the family of borides crystallizing with the $Cr_{23}C_6$-type structure and in Fe_2B.[18] This CN 8 is the same as that found in the new $Ti_2Ru_{2.8}Ir_{2.2}B_3$ phase, but with different polyhedra. Furthermore, the smallest metallic element (beryllium), which is near to boron in the periodic table, although a bit larger, was already found at the same site in the isotypic $A_2BeT_5B_2$ (A = Mg, Sc; T = Rh, Ir)

Table 3. Selected Interatomic Distances d_{ij} (Å) in $Ti_3Ru_{2.9(2)}Ir_{2.1(2)}B_2$, $Ti_{2.63(4)}Ru_{3.4(2)}Ir_{1.6(2)}B_{2.37(4)}$, $Ti_{2.27(6)}Ru_{2.5(2)}Ir_{2.5(2)}B_{2.73(6)}$, and $Ti_2Ru_{2.8(2)}Ir_{2.2(2)}B_3$

		d_{ij}			
site *i*	site *j*	$Ti_3Ru_{2.9}Ir_{2.1}B_2$ (60.1 VE)	$Ti_{2.63}Ru_{3.4}Ir_{1.6}B_{2.37}$ (59.2 VE)	$Ti_{2.27}Ru_{2.5}Ir_{2.5}B_{2.73}$ (59.8 VE)	$Ti_2Ru_{2.8}Ir_{2.2}B_3$ (59.2 VE)
Ru1/Ir1	B1	2.16(2)	2.15(2)	2.17(2)	2.15(2)
	X2[a]	2.568(2)	2.524(1)	2.472(2)	2.401(1)
	Ru2/Ir2	2.715(2)	2.727(2)	2.757(2)	2.746(1)
	Ti1	2.785(5)−2.910(5)	2.775(2)−2.892(3)	2.772(5)−2.882(5)	2.739(3)−2.833(3)
	Ru1/Ir1	2.781(2)−2.972(2)	2.819(2)−2.944(2)	2.816(3)−2.927(2)	2.730(1)−2.941(1)
Ru2/Ir2	B1	2.18(3)	2.20(2)	2.21(3)	2.18(2)
	Ru1/Ir1	2.715(2)	2.727(2)	2.757(2)	2.746(1)
	Ti1	2.736(4)	2.708(3)	2.702(6)	2.664(3)
	Ru2/Ir2	2.972(2)	2.944(2)	2.928(2)	2.855(1)

[a] X2 refers either to Ti2 (in $Ti_3Ru_{2.9}Ir_{2.1}B_2$), to Ti2/B2 (in $Ti_{2.63}Ru_{3.4}Ir_{1.6}B_{2.37}$ and $Ti_{2.27}Ru_{2.5}Ir_{2.5}B_{2.73}$), or to B2 (in $Ti_2Ru_{2.8}Ir_{2.2}B_3$).

dx.doi.org/10.1021/ic102148x |*Inorg. Chem.* 2011, 50, 3332–3341

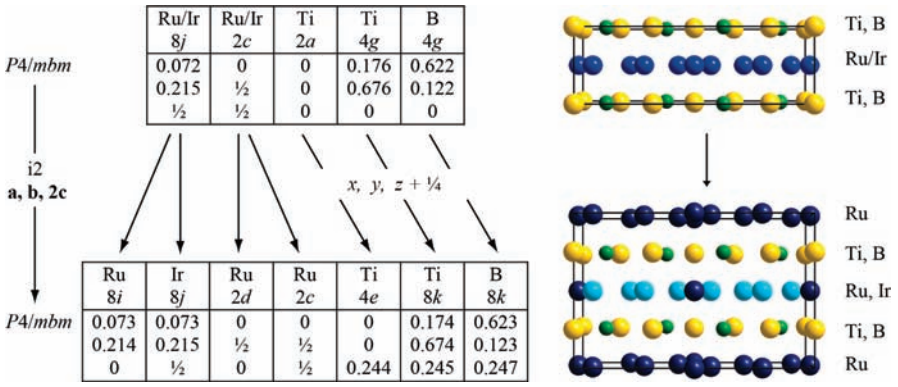

Ru/Ir 8j	Ru/Ir 2c	Ti 2a	Ti 4g	B 4g
0.072	0	0	0.176	0.622
0.215	½	0	0.676	0.122
½	½	0	0	0

Ru 8i	Ir 8j	Ru 2d	Ru 2c	Ti 4e	Ti 8k	B 8k
0.073	0.073	0	0	0	0.174	0.623
0.214	0.215	½	½	0	0.674	0.123
0	½	0	½	0.244	0.245	0.247

Figure 3. Baernighausen tree for the isomorphic transformation from the subcell of $Ti_3Ru_3Ir_2B_2$ to its hypothetical supercell (left scheme). The coordinates of the supercell were obtained from *first-principles* calculations. Details in the boxes: element, Wyckoff position, and atomic coordinates *x*, *y*, *z*. On the right-hand side are the experimental (subcell, top) and theoretical (supercell, bottom) crystal structures highlighting the different layers along [001].

phases.[2,3] All of these hints, together with the fact that titanium has been gradually substituted by boron in the tetragonal prism to produce this complex boride series, indicate indeed that boron can be found in this type of polyhedral environment. Nonetheless, first-principles electronic-structure calculations of the DFT type based on the generalized gradient approximation (GGA) and the projector-augmented-wave (PAW) method have been subsequently performed to probe the stability of this boron-richer phase (see the Theoretical Section).

Homogeneity Ranges. The $Ti_{3-x}Ru_{5-y}Ir_yB_{2+x}$ series is really complex. In fact, it can be thought of as being a set of many independent series.

At constant whole-numbered *x* values ($x = 0, 1$), the series $Ti_3Ru_{5-y}Ir_yB_2$ and $Ti_2Ru_{5-y}Ir_yB_3$ are derived. However, because of the simultaneous filling by ruthenium and iridium of both 2c and 8j sites, as well as the observed Ru/Ir site preference, it will be very difficult to synthesize single-phase products in these two series. In fact, because of the competition between ruthenium and iridium on both sites, a small phase width will always be present, as was observed for the $Ti_3Ru_{2.9}Ir_{2.1}B_2$ and $Ti_2Ru_{2.8}Ir_{2.2}B_3$ phases, which were both synthesized using a Ru/Ir starting ratio of 3:2 (i.e., $y = 2$). Nevertheless, it remains interesting to try to study in the future the homogeneity ranges of both series. Of particular interest will be the end phases $Ti_3Ru_5B_2$, $Ti_3Ir_5B_2$, $Ti_2Ru_5B_3$, and $Ti_2Ir_5B_3$ (i.e., $y = 0, 5$): Are these ternary compounds stable? Can they be synthesized? Some hints from the theoretical calculations already show that these ternary phases are less stable than their quaternary counterparts (see the Theoretical Section). Synthesis of the $Ti_3Ir_5B_2$ phase was attempted, but the desired phase was not achieved because an unexpected phase adopting the cubic perovskite-type structure was obtained, instead. Also, the ruthenium-rich phase $Ti_3Ru_5B_2$ has a stoichiometry near that of the known $Ti_{10}Ru_{19}B_8$ (or $Ti_{2.5}Ru_{4.75}B_2$) phase ($Zn_{11}Rh_{18}B_8$ type), and recalling that the synthesis of $Ti_2FeRu_5B_2$ has produced a phase also of the $Zn_{11}Rh_{18}B_8$ type, instead, indicates that the synthesis of $Ti_3Ru_5B_2$ is unlikely. These findings support the theoretical hints of instability of these ternary phases.

At constant whole-numbered *y* values ($y = n$), the $Ti_{3-x}Ru_{5-n}Ir_nB_{2+x}$ series will be obtained. However, given the fact that it is already difficult to synthesize a single phase at a given whole-numbered *y* value as shown above for $y = 2$ and because the value of *x* is coupled with that of *y*, a more pronounced phase width will be the result. This behavior is observed during the synthesis of $Ti_{2.5}Ru_3Ir_2B_{2.5}$ ($y = 2$, $x = 0.5$), from which two single crystals lead to the formulas $Ti_{2.63}Ru_{3.4}Ir_{1.6}B_{2.37}$ and $Ti_{2.27}Ru_{2.5}Ir_{2.5}B_{2.73}$, confirming the phase width expected for the $Ti_{3-x}Ru_{5-n}Ir_nB_{2+x}$ series and thus making the synthesis of single-phase products here even more difficult.

3. THEORETICAL SECTION

In order to gain more insight into the stability of the boron-richer phase, and in particular the presence of boron in a $(Ir/Ru)_8$ tetragonal prism, we have performed first-principles electronic-structure calculations of the DFT type.

3.1. Theoretical Methodology. *Structural Details.* A structural model was established, using the supercell approach, for the two phases with the chemical formulas $Ti_3Ru_3Ir_2B_2$ and $Ti_2Ru_3Ir_2B_3$. These compositions are very close to those found experimentally, $Ti_3Ru_{2.9}Ir_{2.1}B_2$ and $Ti_2Ru_{2.8}Ir_{2.2}B_3$. The Ru/Ir site preference, found in these phases by single-crystal analysis, has also been modeled using this supercell approach, which implies a doubling of the *c* lattice parameter but maintains the space group in accordance with an isomorphic group−subgroup relationship (see Figure 3). To take into account the Ru/Ir site preference, the 2c and 2d sites in the supercell (formerly the 2c site in the original cell) were assigned to ruthenium alone, but the 8i and 8j sites (formerly the 8j site in the original cell) were assigned respectively to ruthenium and iridium and vice versa. This model is close to the result of single-crystal structural analysis, which shows that the 2c site is mainly occupied by ruthenium, whereas both ruthenium and iridium nearly equally share the 8j site (see Table 2). The model also introduces two different Ru/Ir layers, which allow the positioning of iridium in one of the two layers (see Figure 3, right). These layers are found only along the [001] direction in this structure type.

Vienna Ab Initio Simulation Package (VASP) Calculations. The calculations were carried out by means of the VASP code based on DFT using plane-wave basis sets.[19,20] PAW potentials were used,[21] with the GGA in the parametrization of Perdew, Burke, and Ernzernhof for describing the exchange-correlation potential.[22] A cutoff energy of 500 eV was chosen, and an $8 \times 8 \times 10$ Monkhorst−Pack *k*-point grid[23] for the unit cell containing four formula units was used for integrations within the Brillouin zone. Forces, stress tensors, atomic positions, unit cell shapes, and unit cell volumes were allowed to relax. The convergence criterion of the electronic-structure calculation was set to 1×10^{-6} eV.

Linear Muffin-Tin Orbital (LMTO) Calculations. First-principles scalar-relativistic electronic-structure calculations and chemical-bonding analyses of the optimized structures emanating from VASP calculations were performed by means of the LMTO method.[24] The LMTO calculations were carried out using the tight-binding (TB)

dx.doi.org/10.1021/ic102148x |*Inorg. Chem.* 2011, 50, 3332–3341

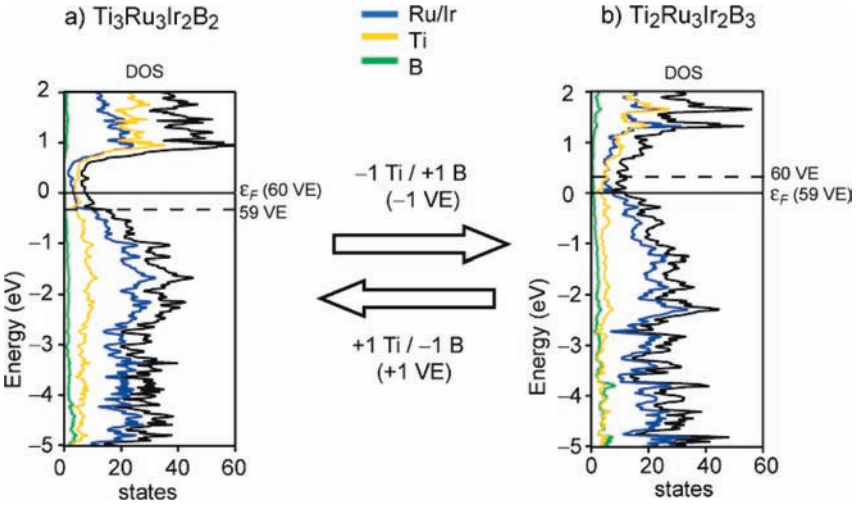

Figure 4. Total (black) and partial DOS curves for $Ti_3Ru_3Ir_2B_2$ (a) and $Ti_2Ru_3Ir_2B_3$ (b) obtained from non-spin-polarized (GGA) calculations. Applying the rigid-band model makes it possible to predict the stability and Fermi level position of one phase relative to another, by removing or adding one valence electron (VE). The Fermi level (E_F) is the energy reference.

representation[25] and the atomic sphere approximation (ASA),[26] as implemented in the STUTTGART TB-LMTO 4.7 program.[27] The electronic energy was calculated via DFT in the GGA method using the Perdew and Wang parametrization of the exchange-correlation potential.[28] A set of 280 irreducible *k* points was needed for Brillouin zone integrations using an improved tetrahedron method.[29] Self-consistency was achieved when the total energy change was smaller than 1×10^{-5} Ry. Chemical-bonding analyses were based on the density of states (DOS) and crystal orbital Hamilton population (COHP) curve.[30]

3.2. Calculation Results and Discussion. *Phase Stability.* The lowest-energy structures calculated (using VASP) for both the $Ti_3Ru_3Ir_2B_2$ and $Ti_2Ru_3Ir_2B_3$ compositions are very similar, and both phases are found to be stable within the $Ti_3Co_5B_2$ structure type. In order to compare the theoretically obtained lattice parameters with the experimental ones, the calculated *c* lattice parameter and the unit cell volume were divided in two. The resulting values are, therefore, $a = 9.315$ Å, $c = 2.989$ Å, and $V = 259.35$ Å^3 for $Ti_3Ru_3Ir_2B_2$ and $a = 9.062$ Å, $c = 2.892$ Å, and $V = 237.49$ Å^3 for $Ti_2Ru_3Ir_2B_3$. Because there are only small differences between the experimental and theoretical compositions (concerning the Ru/Ir ratios), the calculated lattice parameters are very close to the experimental ones (within 1.3%, with the typical GGA overestimation). As expected, the calculated lattice parameters of the boron-richer phase are significantly smaller than those of the boron-poorer one. Consequently, a huge volume difference between both unit cells is obtained; the boron-richer phase has an 8.4% smaller volume. This value is very close to the 8.2% experimentally observed (see Table 1, single-crystal results) and implies, therefore, that both theory and experiment are favorable for a titanium substitution by boron in the $(Ru/Ir)_8$ tetragonal prisms of the $Ti_2Ru_3Ir_2B_3$ phase. This result is further supported by COHP bonding analysis (see below).

Prediction of Phases (Rigid-Band Model). The DOS (using LMTO) for $Ti_3Ru_2Ir_3B_2$ in the valence region involve significant character from all of the elements except boron (Figure 4a). From −5 to ca. −1 eV below the Fermi level (E_F), the DOS exhibits significant ruthenium and iridium character, while titanium and boron levels contribute only slightly. From ca. −1 eV up to E_F, the titanium valence orbitals become more significant. Above E_F, the contribution of the titanium states grows further, resulting in an increase of the overall DOS (Figure 4a). Furthermore, a deep pseudogap is observed between ca. −0.29 and +0.45 eV.

The DOS of $Ti_2Ru_3Ir_2B_3$ is very similar, but its E_F is shifted to lower energy values (Figure 4b). This is the behavior expected from two isotypic phases that closely follow the rigid-band model. In fact, assuming substitution of titanium in $Ti_3Ru_3Ir_2B_2$ by boron en route to $Ti_2Ru_3Ir_2B_3$, the valence electron (VE) count will decrease from 60 VE ($60 = 4 \times 3 + 8 \times 3 + 9 \times 2 + 3 \times 2$ for $Ti_3Ru_2Ir_3B_2$) to 59 VE ($59 = 4 \times 2 + 8 \times 3 + 9 \times 2 + 3 \times 3$ for $Ti_2Ru_3Ir_2B_3$), a process that will induce also a lowering of E_F. Indeed, E_F for $Ti_2Ru_3Ir_2B_3$, estimated from the electronic structure of $Ti_3Ru_3Ir_2B_2$, lies at −0.29 eV and thus is shifted from the middle of the pseudogap to its lower end (see the first part of Table 4 and Figure 4a). The subsequent calculation of the electronic structure of $Ti_2Ru_3Ir_2B_3$ then confirmed the position of its E_F, which is indeed found at the lower end of the pseudogap (see the second part of Table 4 and Figure 4b). This prediction also works if one starts with the electronic structure of $Ti_2Ru_3Ir_2B_3$ and predicts E_F for $Ti_3Ru_3Ir_2B_2$.

Can we predict other isotypic phases containing these four elements using the aforementioned procedure? Because the pseudogaps of both phases are really large, the presence of a phase width is a real possibility, and this corroborates really well with the experimentally found series $Ti_{3-x}Ru_{5-y}Ir_yB_{2+x}$. Starting our phase prediction with the DOS of $Ti_2Ru_3Ir_2B_3$ whose E_F lies at the lower end of the pseudogap, a one VE increment moves E_F to about one-third of the pseudogap, at +0.30 eV, leading, for example, to $Ti_2Ru_2Ir_3B_3$ (if substitution of ruthenium by iridium is assumed) or to $Ti_3Ru_3Ir_2B_2$ (if substitution of boron by titanium in the tetragonal prism is assumed). A further boron substitution by titanium is not possible because the available polyhedron (trigonal prism) is too small for titanium, leaving Ru/Ir substitution as the only feasible possibility to increase the VE. In the next step, two other stable phases may be achieved by a further one VE increment after substitution of ruthenium by iridium, leading to the hypothetical $Ti_2RuIr_4B_3$ and $Ti_3Ru_2Ir_3B_2$ phases and leaving their Fermi levels in the pseudogap (see the second part of Table 4). However, a further VE increment would move the Fermi levels out of the pseudogap, and thus the resulting $Ti_2Ir_5B_3$

Table 4. Possible Phases Predicted from Analyses of the DOS of $Ti_3Ru_3Ir_2B_2$ and $Ti_2Ru_3Ir_2B_3$ Using a Rigid-Band Model[a]

phase	VEC	energy [relative to E_F] (eV)	DOS (states·eV^{-1})
$Ti_3Ir_5B_2$	63	0.84	44.8
$Ti_3RuIr_4B_2/Ti_2Ir_5B_3$	62	0.74	30.9
$Ti_3Ru_2Ir_3B_2/Ti_2RuIr_4B_3$	61	0.45	8.8
$Ti_3Ru_3Ir_2B_2$/$Ti_2Ru_2Ir_3B_3$	**60**	**0.0** (E_F)	**9.9**
$Ti_3Ru_4IrB_2/Ti_2Ru_3Ir_2B_3$	59	−0.29	11.9
$Ti_3Ru_5B_2/Ti_2Ru_4IrB_3$	58	−0.51	23.4
$Ti_2Ru_5B_3$	**57**	−0.66	28.2
$Ti_3Ir_5B_2$	**63**	0.98	23.0
$Ti_2Ir_5B_3/Ti_3RuIr_4B_2$	62	0.81	22.3
$Ti_2RuIr_4B_3/Ti_3Ru_2Ir_3B_2$	61	0.57	13.5
$Ti_2Ru_2Ir_3B_3/Ti_3Ru_3Ir_2B_2$	60	0.30	14.4
$Ti_2Ru_3Ir_2B_3$/$Ti_3Ru_4IrB_2$	**59**	**0.00** (E_F)	**15.7**
$Ti_2Ru_4IrB_3/Ti_3Ru_5B_2$	58	−0.20	21.5
$Ti_2Ru_5B_3$	57	−0.35	22.1

[a] The phases with VEC between 59 and 61 have E_F sitting in the pseudogap and should be more stable than the others. In bold are the calculated phases, from which the others are derived.

and $Ti_3RuIr_4B_2$ phases will be less stable than the aforementioned ones. This type of prediction is also possible when starting with the DOS of $Ti_3Ru_2Ir_3B_2$ (see the first part of Table 4), and it will lead to phases that all belong to the complex boride series $Ti_{3-x}Ru_{5-y}Ir_yB_{2+x}$. All possible phases are regrouped in Table 4, with the corresponding E_F and DOS given relative to those of the initial phases $Ti_3Ru_3Ir_2B_2$ and $Ti_2Ru_3Ir_2B_3$. All stable phases are found to have between 59 and 61 VE. As a direct consequence, the four experimentally obtained phases would have been predicted to all be stable because the VE count of each of them lies in the above given stable VE range (see Table 3). Another direct conclusion from this analysis is that ternary phases will be less stable than quaternaries. All stable phases have nonvanishing DOS at E_F and are therefore predicted to be metallic conductors as expected for these intermetallic compounds.

Bonding Analysis. A chemical-bonding analysis is possible on the basis of the shapes (COHP curves) and integrated values of the COHP curves (ICOHP = integrated value of COHP) for various interatomic interactions in the solid. These results are summarized in Figure 5 and Table 5, with ICOHP values for similar interatomic interactions in related elements and binary compounds included for comparison. In order to be able to compare the calculated distances with those experimentally found, we have averaged all distances where ruthenium and iridium are involved, in particular because they were found to be in the same range. Therefore, the COHP and ICOHP values are analyzed for ruthenium and iridium together (Ru/Ir) and not separately. We will first discuss the bonding situation in the boron-poorer $Ti_3Ru_3Ir_2B_2$ phase and then analyze the influence of titanium substitution by boron en route to the boron-richer $Ti_2Ru_3Ir_2B_3$ phase.

The COHP curves in Figure 5a indicate that the Ru/Ir−B orbital interactions [in the trigonal B(Ru/Ir)$_6$ prisms] are optimized: Bonding orbitals are filled, and antibonding orbitals are empty. The Ru/Ir−Ti orbital interactions [in the tetragonal Ti(Ru/Ir)$_8$ and pentagonal Ti(Ru/Ir)$_{10}$ prisms] are almost optimized in $Ti_3Ru_3Ir_2B_2$. The Ru/Ir−Ru/Ir contacts show antibonding

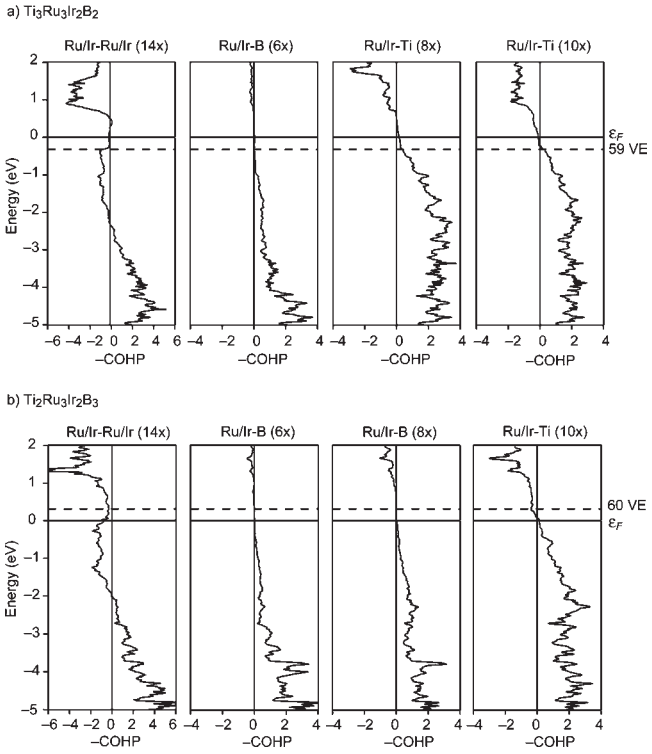

Figure 5. COHP curves for Ru/Ir−Ru/Ir, Ru/Ir−B (B in a trigonal prism), Ru/Ir−Ti (Ti in a tetragonal prism), and Ru/Ir−Ti (Ti in a pentagonal prism) contacts in $Ti_3Ru_3Ir_2B_2$ (a) and for Ru/Ir−B (B in a trigonal prism), Ru/Ir−B (B in a tetragonal prism), and Ru/Ir−Ti (Ti in a pentagonal prism) contacts in $Ti_2Ru_3Ir_2B_3$ (b) from non-spin-polarized (GGA) calculations. The Fermi level (E_F) is the energy reference.

Table 5. Selected Average Distances *d* (Å) and Average ICOHP (eV·bond^{-1}) Values of $Ti_3Ru_3Ir_2B_2$, $Ti_2Ru_3Ir_2B_3$, and Related Examples

		$Ti_3Ru_3Ir_2B_2$		$Ti_2Ru_3Ir_2B_3$		related example		
site *i*	site *j*	*d*	ICOHP	*d*	ICOHP		*d*	ICOHP
M[a]	B	2.186	−2.885	2.185	−2.865	Ru_7B_3	2.175	−2.923
	X[b]	2.587	−2.227	2.412	−1.963	TiRu	2.663	−1.848
	Ti	2.847	−1.464	2.779	−1.522			
	M[a]	2.926	−0.809	2.837	−0.924	Ru (hcp)	2.696	−1.570
						Ir (fcc)	2.742	−1.652

[a] M refers either to Ru/Ir (in $Ti_3Ru_3Ir_2B_2$ and $Ti_2Ru_3Ir_2B_3$), to Ru (in elemental Ru, in Ru_7B_3, and in TiRu), or to Ir (in elemental Ir). [b] X (tetragonal prism site) refers either to Ti (in $Ti_3Ru_3Ir_2B_2$) or to B (in $Ti_2Ru_3Ir_2B_3$).

character just below the Fermi level. This COHP analysis suggests that it is the heteroatomic Ru/Ir−B and Ru/Ir−Ti bonds that are mainly responsible for the structural stability of $Ti_3Ru_3Ir_2B_2$. In agreement with this analysis, the larger ICOHP values are found for the Ru/Ir−B and Ru/Ir−Ti contacts, with those of the Ru/Ir−B distances being the largest (average −2.89 eV·bond^{-1}). The calculated Ru/Ir−B distances (average 2.19 Å) are very close to the experimental ones (average 2.17 Å in $Ti_3Ru_{2.9}Ir_{2.1}B_2$; Table 3). Furthermore, they are just slightly

dx.doi.org/10.1021/ic102148x |*Inorg. Chem.* 2011, 50, 3332–3341

larger than the sum of their covalent radii (2.07 Å for Ru−B and 2.08 Å for Ir−B), thus confirming strong Ru/Ir−B bonding. In comparison, for example, with the ICOHP values for the Ru−B interactions present in Ru_7B_3, $Ti_9M_2Ru_{18}B_8$ (M = Cr−Zn),[12] and $Zr_2FeRu_5B_2$,[6d] in which the boron atoms are also found on trigonal-prismatic coordinated sites, they all lie in the same range (between −2.76 and −2.93 eV·bond^{-1}). The ICOHP values for the Ru/Ir−Ti bonds, −2.23 and −1.46 eV·bond^{-1} found respectively in the tetragonal $Ti(Ru/Ir)_8$ prisms and in the pentagonal $Ti(Ru/Ir)_{10}$ prisms, also indicate significant orbital interactions, with those in the tetragonal prisms being the strongest. The Ru−Ti bonds (2.66 Å) are also found in the $TiRu_8$ tetragonal prisms (cubes) of the intermetallic RuTi compound, but with a 17.1% smaller ICOHP value, indicating much stronger interactions in the tetragonal prisms of the new quaternary phase. However, averaging all of the Ru/Ir−Ti interactions in both types of prisms before comparison has resulted in almost the same ICOHP value like that of the binary RuTi phase, suggesting the presence of similar bonding strength in the two phases. Furthermore, the calculated average Ru/Ir−Ti bonds are in very good agreement with the experimentally found average ones (see Tables 3 and 5). The consequence of these strong heteroatomic Ru/Ir−B and Ru/Ir−Ti interactions is that the homoatomic Ru/Ir−Ru/Ir, Ti−Ti, and B−B will be weakened. Indeed the average ICOHP value found for Ru/Ir−Ru/Ir is significantly smaller than those found in the corresponding elements (see Table 5), and the remaining homoatomic Ti−Ti and B−B are too weak to be considered as bonding.

Let us now switch to the boron-richer phase, $Ti_2Ru_3Ir_2B_3$, and compare its bonding situation with the aforementioned $Ti_3Ru_3Ir_2B_2$. The only main structural difference between both phases resides in the tetragonal $(Ru/Ir)_8$ prisms, which are filled by boron in the former but by titanium in the latter. In accordance with this structural fact, the COHP curves and the ICOHP values of both phases show significant differences only for the heteroatomic interactions within these tetragonal prisms (see Figure 5 and Table 5). In fact, the overall shape of the COHP curve for the Ru/Ir−B orbital interactions [in the tetragonal $B(Ru/Ir)_8$ prisms] is rightly different from that of the corresponding Ru/Ir−Ti interactions, given the totally different electronic nature of titanium and boron. However, both COHP curves are optimized, suggesting that boron, indeed, also has significant orbital interactions with Ru/Ir in the tetragonal prisms. This is further supported by the fact that its ICOHP value is found to be the second highest of all interactions in the $Ti_2Ru_3Ir_2B_3$ phase, just behind that of the same type of interactions but which are found within trigonal $B(Ru/Ir)_6$ prisms (see Table 5). It is worth mentioning that the calculated Ru/Ir−B bond in the tetragonal $B(Ru/Ir)_8$ prisms is very close (only 0.4% overestimation) to the experimental value. This indicates that both theory and experiment are in good agreement with the bonding situation of boron in this tetragonal-prismatic environment of transition metals.

Phase Prediction via COHP Analysis. The substitution of titanium by boron in $Ti_3Ru_3Ir_2B_2$, i.e., the removal of one VE, merely shifts the Fermi level from the 60 VE position to the 59 VE one (see the dashed line in Figure 5a). Indeed, the new position corresponds to that of the calculated Fermi level for the $Ti_2Ru_3Ir_2B_3$ phase (see the solid line in Figure 5b). The opposite prediction (starting from the COHP curve of $Ti_2Ru_3Ir_2B_3$) also leads to the correct determination of the Fermi level of $Ti_3Ru_3Ir_2B_2$ (see the dashed line in Figure 5b). This method may even be used to predict other stable phases as was done above for DOS analysis. In fact, the COHP curves of the strongest interactions in both phases show around the Fermi level a wide range of energies with nonbonding orbitals. Therefore, shifting the Fermi level within this energy range will result in new electronically different phases but with nearly the same stability, in terms of the strongest bonding interactions.

4. CONCLUSIONS

The first transition-metal borides in the Ti−Ru−Ir−B system, in the form of the complex boride series $Ti_{3-x}Ru_{5-y}Ir_yB_{2+x}$, have been studied experimentally and theoretically. They were synthesized by arc-melting the elements and characterized by single-crystal X-ray analysis as well as WDS and EDS measurements. They crystallize as new substitutional variants of the $Ti_3Co_5B_2$-type structure, and a strong Ru/Ir site preference is observed. In addition to finding boron in the usual trigonal-prismatic coordination, boron is also found for the first time within an 8-fold tetragonal-prismatic coordination in the $Ti_2Ru_{2.8}Ir_{2.2}B_3$ phase. DFT calculations have not only confirmed the stability of these phases but also show that the Ru/Ir−B and Ru/Ir−Ti heteroatomic interactions are mainly responsible for their structural stability. These calculations further predict, via the rigid-band model, many other possible quaternary phases of the aforementioned complex boride series to be more stable than their ternary counterparts.

■ ASSOCIATED CONTENT

Supporting Information. Crystallographic information files (in CIF format), Rietveld refinement plot of the $Ti_3Ru_3Ir_2B_2$ product (Figure S1), and the indexed powder diffraction data for $Ti_3Ru_3Ir_2B_2$ (Table S1) and $Ti_2Ru_3Ir_2B_3$ (Table S2). This material is available free of charge via the Internet at http://pubs.acs.org.

■ AUTHOR INFORMATION

Corresponding Author

*E-mail: boniface.fokwa@ac.rwth-aachen.de. Tel.: +49 (0) 241 80-94655. Fax: +49 (0) 241 80-92642.

■ ACKNOWLEDGMENT

The Deutsche Forschungsgemeinschaft is gratefully acknowledged for financial support through the Heisenberg fellowship awarded to BPT Fokwa. We also thank Klaus Kruse for various X-ray data collections, Resi Zaunbrecher (IPC, RWTH-Aachen) for the EDS analyses, and Dr. Silvia Richter and Jens Schulz-Kuhnert for the various time-consuming WDS analyses.

■ REFERENCES

(1) Kuz'ma, Yu. B.; Yarmolyuk, Ya. P. *Zh. Strukt. Khim.* **1971**, *12*, 458.
(2) Jung, W.; Schiffer, J. *Z. Anorg. Allg. Chem.* **1990**, *581*, 135.
(3) Nagelschmitz, E. A.; Jung, W. *Chem. Mater.* **1998**, *10*, 3189.
(4) Nagelschmitz, E. A.; Jung, W.; Feiten, R.; Müller, P.; Lueken, H. *Z. Anorg. Allg. Chem.* **2001**, *627*, 523.
(5) (a) Dronskowski, R.; Korczak, K.; Lueken, H.; Jung, W. *Angew. Chem.* **2002**, *114*, 2638; *Angew. Chem., Int. Ed.* **2002**, *41*, 2528.
(6) (a) Fokwa, B. P. T.; Lueken, H.; Dronskowski, R. *Chem.—Eur. J.* **2007**, *13*, 6040. (b) Samolyuk, G. D.; Fokwa, B. P. T.; Dronskowski, R.; Miller, G. J. *Phys. Rev. B* **2007**, *76*, 094404. (c) Fokwa, B. P. T. *Eur. J. Inorg. Chem.* **2010**, 3075. (d) Brgoch, J.; Yeninas, S.; Prozorov, R.; Miller, G. J. *J. Solid State Chem.* **2010**, *183*, 2917.

(7) Alekseeva, A. M.; Abakumov, A. M.; Chizhov, P. S.; LeitheJasper, A.; Schnelle, W.; Prots, Yu.; Hadermann, J.; Antipov, E. V.; Grin, Yu. *Inorg. Chem.* **2007**, *46*, 7378.
(8) *WinXPOW*, version 1.06; STOE Cie: Darmstadt, Germany, 1999.
(9) Sheldrick, G. M. *SADABS*; University of Göttingen: Göttingen, Germany, 2001.
(10) Sheldrick, G. M. *Acta Crystallogr.* **2008**, *A64*, 112.
(11) Gelato, L. M.; Parthé, E. *J. Appl. Crystallogr.* **1987**, *20*, 139.
(12) Fokwa, B. P. T. *Z. Anorg. Allg. Chem.* **2009**, *635*, 2258.
(13) (a) Fokwa, B. P. T.; Samolyuk, G. D.; Miller, G. J.; Dronskowski, R. *Inorg. Chem.* **2008**, *47*, 2113. (b) Fokwa, B. P. T.; Goerens, C.; Gillessen, M. *Z. Kristallogr.* **2010**, *225*, 180.
(14) Fokwa, B. P. T.; von Appen, J.; Dronskowski, R. *Chem. Commun.* **2006**, 4419.
(15) Rogl, P.; Benesovsky, F.; Nowotny, H. *Monatsh. Chem.* **1972**, *103*, 965.
(16) Vandenberg, J. M.; Matthias, B. T.; Corenzwit, E.; Barz, H. *Mater. Res. Bull.* **1975**, *10*, 889.
(17) (a) Salamakha, P.; Goncalves, A. P.; Sologub, O. L.; Almeida, M. *J. Alloys Compd.* **2003**, *360*, 61. (b) Kluenter, W.; Jung, W. *Z. Anorg. Allg. Chem.* **1995**, *621*, 197. (c) Zaikina, J. V.; Jo, Y.-J.; Latturner, S. E. *Inorg. Chem.* **2010**, *49*, 2773.
(18) Villars, P.; Cenzual, K. *Pearson's Crystal Structure Database for Inorganic Compounds (on CD-ROM)*, version 1.0; ASM International: Materials Park, OH, 2007/2008.
(19) (a) Kresse, G.; Furthmüller, J. *Comput. Mater. Sci.* **1996**, *6*, 15. (b) Kresse, G.; Furthmüller, J. *Phys. Rev. B* **1996**, *55*, 11169.
(20) (a) Kresse, G.; Hafner, J. *Phys. Rev. B* **1993**, *47*, 558. (b) Kresse, G.; Hafner, J. *Phys. Rev. B* **1994**, *49*, 14251.
(21) Blöchl, P. E. *Phys. Rev. B* **1994**, *50*, 17953.
(22) Perdew, J. P.; Burke, K.; Ernzerhof, M. *Phys. Rev. Lett.* **1996**, *77*, 3865.
(23) Monkhorst, H. J.; Pack, J. D. *Phys. Rev. B* **1976**, *13*, 5188.
(24) (a) Andersen, O. K.; Jepsen, O. *Phys. Rev. B* **1975**, *12*, 3060. (b) Skriver, H. L. *The LMTO Method*; Springer-Verlag: Berlin, 1984. (c) Andersen, O. K. In . *Proceedings of a NATO Advanced Study Institute*; Phariseau, P., Temmermann, W. H., Eds.; Plenum Press: New York, 1984; pp 11−66.
(25) Andersen, O. K.; Jepsen, O. *Phys. Rev. Lett.* **1984**, *53*, 2571.
(26) Andersen, O. K.; Skriver, H.; Nohl, H.; Johansson, B. *Pure Appl. Chem.* **1980**, *52*, 93.
(27) Jepsen, O.; Andersen, O. K. *The STUTTGART TB-LMTO Program*; Max-Planck-Institut für Festkörperforschung: Stuttgart, Germany, 2000.
(28) Perdew, J. P.; Wang, Y. *Phys. Rev. B* **1992**, *45*, 13244.
(29) Blöchl, P. E.; Jepsen, O.; Andersen, O. K. *Phys. Rev. B* **1994**, *49*, 16223.
(30) Dronskowski, R.; Blöchl, P. E. *J. Phys. Chem.* **1993**, *97*, 8617.